

PAPER • OPEN ACCESS

The effect of particle density on ultrasound-mediated transport of nanoparticles

To cite this article: Harriet Lea-Banks *et al* 2016 *Phys. Med. Biol.* **61** 7906

View the [article online](#) for updates and enhancements.

Related content

- [Cavitation-enhanced delivery of insulin in agar and porcine models of human skin](#)
Helga Feiszthuber, Sunali Bhatnagar, Miklós Gyöngy *et al.*
- [Passive acoustic mapping of magnetic microbubbles for cavitation enhancement and localization](#)
Calum Crake, Marie de Saint Victor, Joshua Owen *et al.*
- [Superharmonic microbubble Doppler effect in ultrasound therapy](#)
Antonios N Poulipoulos and James J Choi

Recent citations

- [Drug Delivery Strategies for Platinum-Based Chemotherapy](#)
Richard J. Browning *et al*

The effect of particle density on ultrasound-mediated transport of nanoparticles

Harriet Lea-Banks¹, Boon Teo, Eleanor Stride
and Constantin C Coussios

Department of Engineering Science, Institute of Biomedical Engineering, University of Oxford, Old Road Campus Research Building, Oxford OX3 7DQ, UK

E-mail: harriet.lea-banks@eng.ox.ac.uk

Received 8 July 2016, revised 25 August 2016

Accepted for publication 29 September 2016

Published 25 October 2016



Abstract

A significant barrier to successful drug delivery is the limited penetration of nanoscale therapeutics beyond the vasculature. Building on recent *in vivo* findings in the context of cancer drug delivery, the current study investigates whether modification of nanoparticle drug-carriers to increase their density can be used to enhance their penetration into viscoelastic materials under ultrasound exposure. A computational model is first presented to predict the transport of identically sized nanoparticles of different densities in an ultrasonic field in the presence of an oscillating microbubble, by a combination of primary and secondary acoustic radiation forces, acoustic streaming and microstreaming. Experiments are then described in which near monodisperse (polydispersity index <0.2) nanoparticles of approximate mean diameter 200 nm and densities ranging from 1.01 g cm^{-3} to 5.58 g cm^{-3} were fabricated and delivered to a tissue-mimicking material in the presence or absence of a microbubble ultrasound contrast agent, at ultrasound frequencies of 0.5 MHz and 1.6 MHz and a peak negative pressure of 1 MPa. Both the theoretical and experimental results confirm that denser particles exhibit significantly greater ultrasound-mediated transport than their lower density counterparts, indicating that density is a key consideration in the design of nanoscale therapeutics.

¹ Author to whom any correspondence should be addressed.



Original content from this work may be used under the terms of the [Creative Commons Attribution 3.0 licence](https://creativecommons.org/licenses/by/3.0/). Any further distribution of this work must maintain attribution to the author(s) and the title of the work, journal citation and DOI.

Keywords: ultrasound, cavitation, microstreaming, nanoparticles, density, drug delivery

(Some figures may appear in colour only in the online journal)

1. Introduction

Cancerous tissue is highly heterogeneous in terms of perfusion and the pressure and composition of the extracellular matrix, posing a number of significant barriers to drug delivery. Consequently, current methods of systemic drug delivery often do not enable therapeutics to penetrate sufficiently deep into tumour tissue for effective treatment (Minchinton *et al* 2006). This is particularly problematic for relatively large therapeutics such as nanoparticles. Strategies for enhancing the transport of nanoscale drug carriers have included modifying their size, shape and surface chemistry - primarily surface charge and biological targeting (Blanco *et al* 2015). Tailoring the size and shape of nanoparticles can increase their ability to pass through pores in the 'leaky' vasculature that is characteristic of cancerous blood vessels and to be retained in the surrounding tumour tissue—an effect known as enhanced permeability and retention (EPR) (Maeda 2010, Prabhakar *et al* 2013). Exploiting the EPR effect in this way is classified as passive targeting. In contrast, using surface charge or ligands to enable particles to bind to specific receptors on cancer or endothelial cells is classed as active targeting (Kamaly *et al* 2012).

It has been shown that neither passive (Popović *et al* 2010) nor active targeting alone can provide significant enhancements in nanoparticle delivery (Wilhelm *et al* 2016). In combination with physical stimuli, however, much greater penetration depths can be achieved. These stimuli include magnetic fields (Lübbe *et al* 2001), electromagnetic radiation (Dougherty *et al* 1992) and ultrasound. Of these, ultrasound has been shown to achieve the greatest penetration depths and has the advantage of being cost-effective and already clinically approved as an imaging and therapeutic modality (Mo *et al* 2012). The combination of a nanoparticle with microbubbles driven in a sustained inertial cavitation regime has shown promise as a means of enhancing transport, enabling the delivery of nanoparticulate therapeutics to some 200 μm from the nearest blood vessel (Carlisle *et al* 2013). Although size and shape modifications have been heavily explored, relatively little attention has been given to the influence of particle density on the delivery and penetration distance of nanoscale drug carriers when exposed to ultrasound.

It has been shown previously that coating an adenovirus of mean size 140 nm with gold nanoparticles can enhance its ultrasound-mediated transport in a mouse model in the presence of a microbubble ultrasound contrast agent (Mo *et al* 2015). It was hypothesised that this enhancement was due to the polymer-gold coating providing both reduced immunogenicity, and hence increased circulation time, and an increase in density that facilitates transport by cavitation microstreaming. The current study aims to test this hypothesis and to determine how the ultrasound-mediated transport of a nanoscale object is affected by its density. Additionally, the influence of ultrasound exposure conditions and the incidence of cavitation will also be examined.

2. Numerical model

2.1. Methodology

A simple computational model was first developed to compare the magnitude of the different forces acting on a 200 nm diameter nanoparticle suspended in water and subjected to an ultrasound field, under different exposure conditions, in the presence or absence of a 3 μm

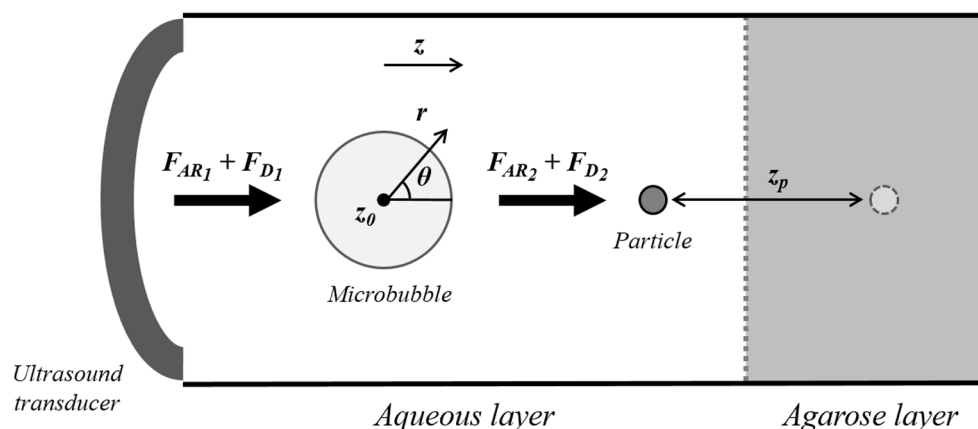


Figure 1. Schematic of the model-system used to estimate the primary acoustic radiation force (F_{AR1}), acoustic streaming force (F_{D1}), secondary radiation force (F_{AR2}) and microstreaming force (F_{D2}) on a 200 nm solid particle in aqueous suspension, and predict the resultant penetration distance (z_p).

diameter microbubble. This model was then used to predict the distance that the particle would travel beyond a planar water/agarose boundary into agarose gel. Agarose was used here both in the computational and experimental models as a tissue-mimicking material, having similar density, acoustic properties and pore size to those of human tissue (Maaloum *et al* 1998). A particle size of 200 nm was chosen as being representative of larger nanoparticulate therapeutics, such as viruses or liposomes, whilst still being small enough to extravasate through leaky tumour vasculature (Hobbs *et al* 1998).

A schematic of the system is shown in figure 1. In the absence of the microbubble, the particle will experience an acoustic radiation force (F_{AR1}) due to the propagating ultrasound field and a second force due to acoustic streaming (F_{D1}). The latter was calculated using Stoke's equation for drag (equation (1)). This was deemed to be justified since the regimes considered relate to a nanoscale object and low streaming velocities, on the order of cm s^{-1} , producing Reynolds numbers on the order of 1×10^{-3} .

In the presence of the microbubble, the particle will experience two additional forces: a secondary acoustic radiation force (F_{AR2}) and a force due to microstreaming (F_{D2}). The response of a 3 μm diameter microbubble in free-field conditions was modelled using the Keller–Miksis equation (equation (2)) (Keller *et al* 1980), and the predicted radial oscillations for driving frequencies of 0.5 MHz and 1.6 MHz and a peak negative pressure of 1 MPa are shown in figure 2. To account for the sulphur hexafluoride encapsulated inside SonoVue® (Bracco Imaging, France) contrast agent microbubbles used in the experiments, a specific heat ratio (γ) of 1.098 was used to describe the internal gas (Schneider *et al* 1995). The effect of the microbubble coating was neglected in order to simplify the model. Initial simulations (appendix) indicated that the influence of the coating on microbubble dynamics, for the ultrasound exposure parameters used in the study, was negligible. The scattered pressure field was calculated from the corresponding potential flow (equation (3)) (Ilinskii 1992), which was in turn used to determine the magnitude of the secondary radiation force. The microstreaming model published by Doinikov (2010) was implemented to assess the velocity field around the microbubble (equation (32), Doinikov 2010). The radial component of microstreaming taken in the positive ' r ' direction (i.e. towards the water/agar boundary) was used to determine the corresponding force on the particle that would lead to penetration into the agar, again assuming Stoke's drag.

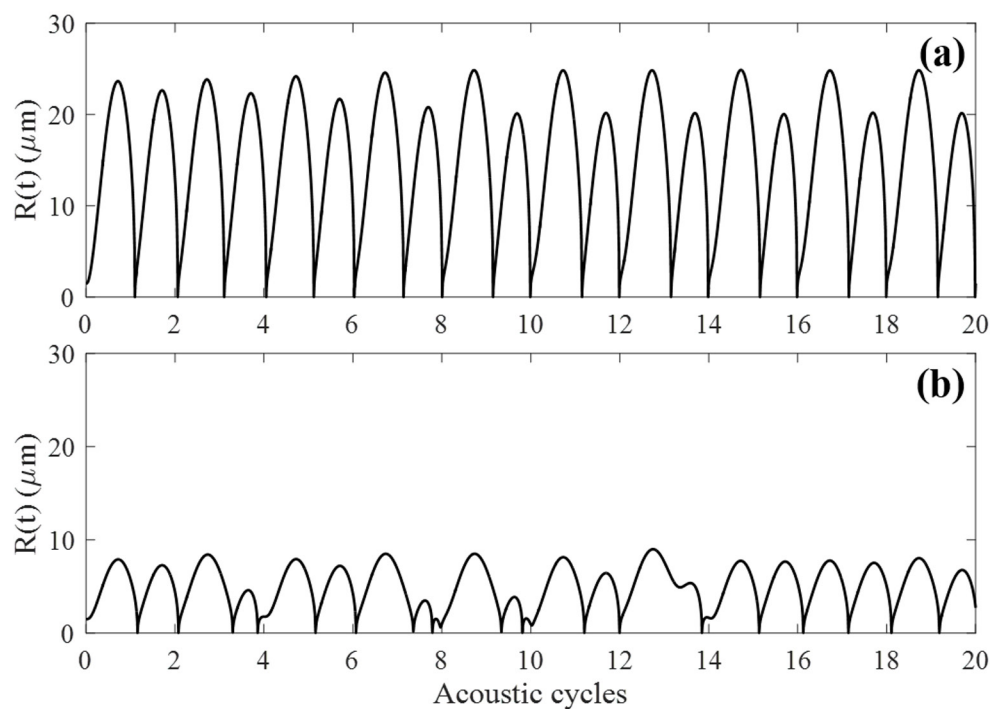


Figure 2. Radius-time curves predicted by the Keller–Miksis model for the dynamic response of a $3\text{ }\mu\text{m}$ bubble driven at 1 MPa at (a) 0.5 MHz and (b) 1.6 MHz for the first 20 acoustic cycles.

Table 1. Predicted force magnitudes on a 200 nm solid particle at a distance of twice the viscous penetration depth from the surface of an oscillating $3\text{ }\mu\text{m}$ bubble at a peak negative pressure of 1 MPa.

	1.6 MHz + SV	0.5 MHz + SV
Primary acoustic radiation force (F_{AR1})	$5.0 \times 10^{-13}\text{ N}$	$7.7 \times 10^{-14}\text{ N}$
Acoustic streaming force (F_{D1})	$8.1 \times 10^{-11}\text{ N}$ ($u_1 = 4.31\text{ cm s}^{-1}$)	$7.8 \times 10^{-13}\text{ N}$ ($u_1 = 0.41\text{ cm s}^{-1}$)
Secondary acoustic radiation force (F_{AR2})	$1.7 \times 10^{-11}\text{ N}$	$1.4 \times 10^{-11}\text{ N}$
Microstreaming force (F_{D2})	$2.9 \times 10^{-10}\text{ N}$ ($u_2 = 15.4\text{ cm s}^{-1}$)	$6.3 \times 10^{-10}\text{ N}$ ($u_2 = 33.6\text{ cm s}^{-1}$)

The relative magnitudes of the four forces acting on the particle are shown in table 1. These values illustrate that within therapeutically relevant acoustic regimes, such as 0.5 MHz and 1.6 MHz in which the bubble is excited at or below resonance, the greatest of the four forces is provided by the microstreaming. Since depth of penetration was the primary quantity of interest, only the z -axis component of these forces was considered. The nanoparticle was assumed to be located initially at a distance of twice the viscous penetration depth from the bubble outer surface (equation (4)) (Doinikov 2010) and to be travelling at the velocity of the fluid by the time it had reached the aqueous/agarose boundary (equation (5)). The effective particle mass

accounts for the mass of the particle and the added mass due to the inertia of the displaced fluid (equation (6)). Penetration depth into the agarose gel was predicted using a non-Newtonian fluid model (equation (7)) (de Bruyn *et al* 2004), in which agarose viscosity and yield strength are free parameters that may be determined from experimental observations. Since published parameters vary considerably however, for the purposes of this study, the predicted penetration depths were normalised to the peak penetration depth found across any of the ultrasound exposure conditions, with the maximum normalised value being 1000.

$$F_{D1} = 6\pi R_p \mu (u_1 - v_p), \quad F_{D2} = 6\pi R_p \mu (u_2 - v_p) \quad (1)$$

where u_1 and u_2 are determined from the microstreaming model (Doinikov 2010)

$$\begin{aligned} \ddot{R} = & \left(\frac{1}{2} \dot{R}^3 + \dot{R} \Delta(R) - c \left(\frac{3}{2} \dot{R}^2 + \frac{4\mu \dot{R}}{\rho_L R} + \frac{2\sigma}{\rho_L R} - \Delta(R) \right) + R \dot{R} \Delta'(R) \right. \\ & \left. + \left(1 + \frac{\dot{R}}{c} \right) \frac{P_a c}{\rho_L} \sin \omega \left(t + \frac{R}{c} \right) \right) \left(\frac{4\mu}{\rho_L} - R(\dot{R} - c) \right)^{-1} \\ & \text{where } \Delta(R) = \left(\left(p_0 + \frac{2\sigma}{R_0} \right) \left(\frac{R_0}{R} \right)^{3\gamma} - p_0 \right) \rho_L^{-1} \end{aligned} \quad (2)$$

$$p_{\text{scat}} = \frac{\rho_L R}{r} (R \ddot{R} + 2 \dot{R}^2) \quad (3)$$

$$r = R_0 + 2\delta_v, \text{ where } \delta_v = \sqrt{2\mu/\rho_L \omega} \quad (4)$$

$$v_p = (u_1 + u_2) \quad (5)$$

$$m = m_p + m_{\text{added}} = \frac{4}{3} \pi R_p^3 \rho_p + \frac{2}{3} \pi R_p^3 \rho_L \quad (6)$$

$$\delta_p = \frac{mv_p}{k} - \frac{F_y m}{k^2} \ln \left(1 + \frac{v_p k}{F_y} \right) \quad (7)$$

Variables

F_{AR1}	Acoustic radiation force	R	Instantaneous radius
F_{AR2}	Secondary acoustic radiation force	\dot{R}	Radial velocity
F_{D1}	Acoustic streaming force	\ddot{R}	Radial acceleration
F_{D2}	Microstreaming force	R_p	Particle radius
F_y	Yield stress force of agarose	u_1	Acoustic streaming velocity
k	Effective viscous drag	u_2	Microstreaming velocity
m	Effective particle mass	v_p	Particle velocity
m_{added}	Added mass	δ_p	Particle penetration depth
m_p	Particle mass	δ_v	Viscous penetration depth
P_a	Acoustic pressure	ρ_p	Particle density
r	Initial particle location	ω	Acoustic angular frequency

Constants

c	Sound speed in surrounding medium	1480 m s^{-1}
p_0	Static pressure	$1 \times 10^5 \text{ Pa}$
R_0	Initial bubble radius	$1.5 \mu\text{m}$
R_p	Particle radius	100 nm
ρ_L	Liquid density	1000 kg m^3
μ	Liquid viscosity	0.001 kg ms
σ	Surface tension	0.0725 N m
γ	Ratio of specific heats	1.098

2.2. Results

The penetration depth is predicted for particles of three different densities, with cores of polystyrene (PS), silica (SiO_2) and gold (Au) and a polymer coating, giving final particle densities of 1.01 g cm^{-3} , 1.41 g cm^{-3} and 5.58 g cm^{-3} respectively, under four acoustic regimes (figure 3). The first two acoustic regimes correspond to the case in which no cavitation nuclei are present. Therefore the particle is driven only by the primary acoustic radiation force (F_{AR1}) and the force due to acoustic streaming (F_{D1}). In this non-cavitation regime the model predicts greater penetration depths at 1.6 MHz compared to 0.5 MHz. This is as expected because at higher frequencies the ultrasound energy is more likely to be attenuated by the surrounding fluid, transferring more momentum from the propagating wave to the fluid, in turn inducing greater acoustic streaming velocities. Even at the higher frequency, however, the predicted penetration depth is relatively small compared to that observed with a microbubble present.

When an oscillating microbubble is introduced, much greater penetration depths are predicted for all three types of particle. For example, the greatest predicted penetration depth

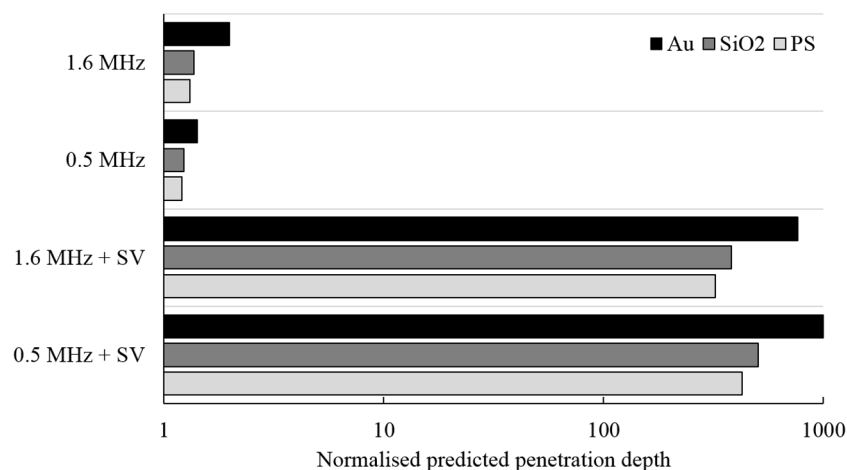


Figure 3. Normalised predicted penetration depths of 200 nm particles of three different densities ($\text{Au} = 5.58 \text{ g cm}^{-3}$, $\text{SiO}_2 = 1.41 \text{ g cm}^{-3}$, $\text{PS} = 1.01 \text{ g cm}^{-3}$) under ultrasound exposure in four acoustic regimes with and without a SonoVue® (SV) microbubble. A microbubble diameter of $3 \mu\text{m}$ was used and a peak negative pressure of 1 MPa over 100 acoustic cycles. Predicted depths are normalised to the peak penetration depth in any of the acoustic regimes, i.e. Au at 0.5 MHz + SV, which was assigned the value 1000 for convenience of display.

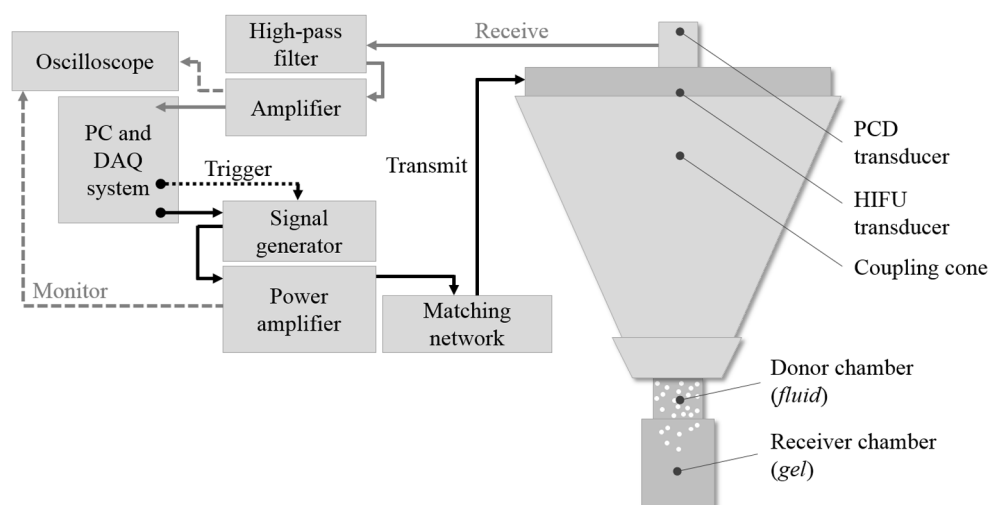


Figure 4. Schematic representation of ultrasound transmit, trigger, receive and monitor circuit; with high-intensity focused ultrasound (HIFU) transducer and passive cavitation detection (PCD) transducer. The coupling cone, filled with degassed water, allows transmission of ultrasound from the HIFU transducer into the donor chamber, filled with fluid, nanoparticles and SonoVue® (SV). Nanoparticles are transported from the donor chamber to the receiver chamber, filled with agarose gel.

achieved by the gold nanoparticle without cavitation is 0.2% of the greatest predicted penetration depth achieved by the gold nanoparticle with cavitation. In this cavitation regime the particles experience the additional secondary acoustic radiation force (F_{AR2}) and the force generated by microstreaming (F_{D2}). With cavitation nuclei at 0.5 MHz, the predicted penetration depths are greater for all three particles than in the 1.6 MHz regime. As shown in figure 2(a), at 0.5 MHz the 3 μm bubble experiences a longer negative pressure phase than at 1.6 MHz (figure 2(b)), and is therefore able to achieve greater expansion ratios which are associated with greater microstreaming velocities (table 1).

3. Experimental investigations

3.1. Methodology

Ultrasound-mediated transport of contrasting-density nanoparticles was investigated experimentally using the apparatus shown in figure 4, building on similar experimental setups used in previous studies (Bhatnagar *et al* 2014). A high-intensity focussed ultrasound (HIFU) transducer (H-107F-18; Sonic Concepts, USA) with fundamental frequency 0.5 MHz and third harmonic 1.6 MHz was used, allowing two contrasting acoustic regimes to be studied with the same experimental setup. Ultrasound was delivered at a pulse repetition frequency of 10 Hz and 2% duty cycle, with pulse repetition period of 100 ms over a total exposure time of 10 s. Transmission of ultrasound from the HIFU transducer to the aqueous sample of nanoparticles was achieved using a Perspex coupling cone containing degassed deionised (DI) water. Average cavitation signals were captured using a passive cavitation detection (PCD) transducer (V319; Panametrics, Olympus NDT UK Ltd, England) coaxially aligned with the HIFU transducer. High-pass filtering at 5 MHz was implemented to remove the driving signal from the PCD signal. The ‘donor’ chamber, a Perspex cylinder with diameter 12 mm and internal

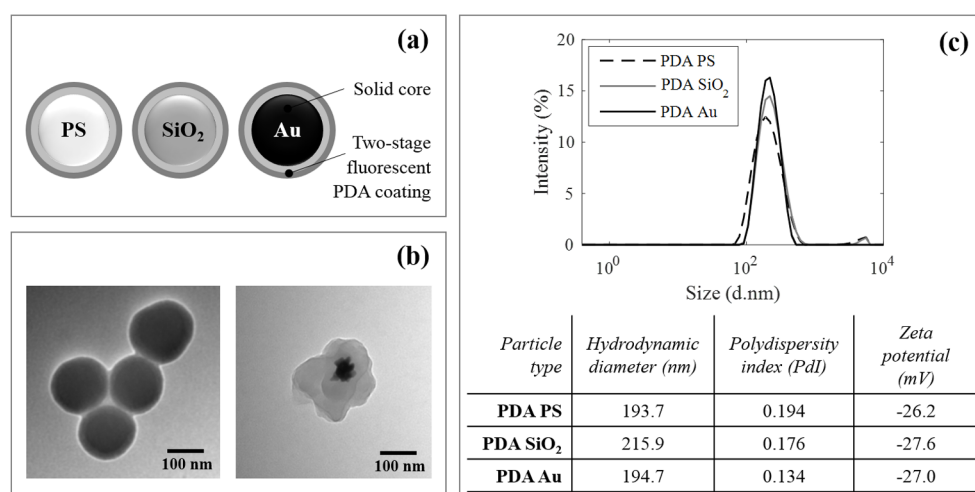


Figure 5. Bespoke density-modified nanoparticles formed from contrasting density cores of polystyrene (PS), silica (SiO₂) or gold (Au) with a fluorescent poly-dopamine (PDA) coating. Particles are shown as (a) a schematic illustration and (b) a transmission electron microscopy (TEM) image of PDA-PS (left) and PDA-Au (right). The size distribution of each particle type is shown in (c) as measured by dynamic light scattering (DLS).

volume of 1.7 ml, was placed beneath the coupling cone and filled with each population of density-contrasting nanoparticles in aqueous suspension and SonoVue® (SV) microbubbles. Nanoparticles were transported from the donor chamber into the receiver chamber, which was filled with a volume of 1% concentration (wt%) agarose gel.

Bespoke density-modified nanoparticles were fabricated using a 100 nm diameter core of polystyrene (PS), silica (SiO₂) or gold (Au), coated with a poly-dopamine (PDA) shell in a two phase coating procedure described by Chen *et al* (2014). The final coated nanoparticles had a diameter of 200 nm and were similar in terms of size distribution (PdI 0.17 ± 0.03), surface charge ($-27 \text{ mV} \pm 2$) and fluorescence (excitation 400 nm, emission 480 nm), but contrasting in density (PDA-PS 1.10 g cm^{-3} , PDA-SiO₂ 1.41 g cm^{-3} , PDA-Au 5.58 g cm^{-3}) (figure 5).

The agarose sample was removed from the receiver chamber and prepared for microscopy, as illustrated in figure 6. Confocal microscopy was used to capture a volumetric scan of the sample. These data were then processed by applying a thresholding function to detect the location of each particle. By locating each particle and measuring the distance from the agarose boundary, a value for penetration depth was obtained. Statistical significance was assessed using analysis of variance (ANOVA), comparing the variation between groups with the variation within groups, and was felt to be a more robust measure than a simple *t* test. A *p*-value < 0.05 was used to disprove the null hypothesis (table 2).

3.2. Results

Figure 7 shows the results from three sets of experiments. In the absence of ultrasound exposure, the average penetration by diffusion alone was limited to less than 30 μm . In the presence of acoustic excitation, the penetration depth exceeded 80 μm in all cases. It can be seen that in each of the acoustic regimes the penetration depth was greatest for the densest particle.

A significant difference can also be seen between the cavitation and non-cavitation regimes; the presence of SV microbubbles significantly enhanced the penetration depths of

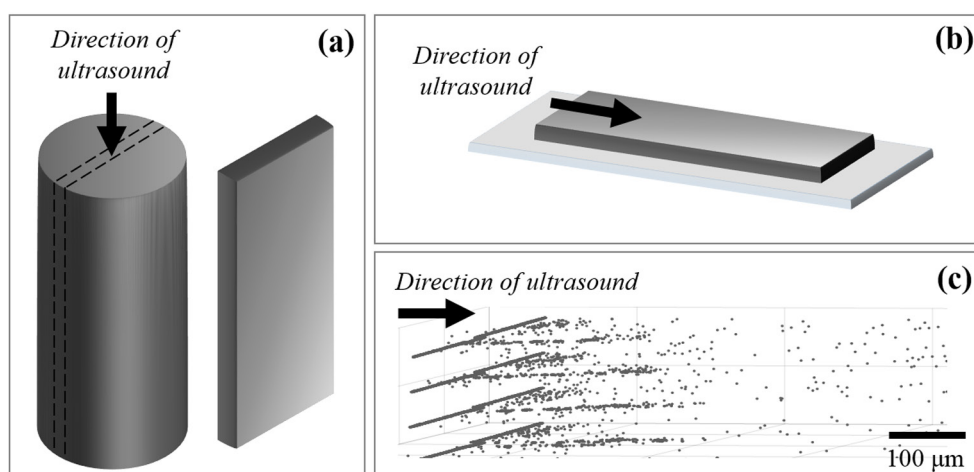


Figure 6. Schematic representation of (a) gel sample and (b) preparation for confocal microscopy by slicing the central plane and applying to a microscope slide. Confocal microscopy was used to obtain (c) a volumetric scan of the sample and particle detection to locate and map the distribution of nanoparticles.

Table 2. Statistical significance and *p*-values assessed through one-way ANOVA testing.

Groups compared		
Group 1	Group 2	<i>p</i> -value
Diffusion Au	0.5 MHz + SV Au	4.09×10^{-5}
Diffusion Au	1.6 MHz + SV Au	0.04
Diffusion SiO₂	0.5 MHz + SV SiO₂	0.06
0.5 MHz Au	0.5 MHz + SV Au	0.02
0.5 MHz + SV Au	0.5 MHz + SV PS	0.05

all particles. An ultrasound frequency of 0.5 MHz was found to be most favourable for particle transport when compared to exposure at 1.6 MHz, in agreement with the theoretical predictions. Figure 8 shows the frequency composition of averaged PCD data during ultrasound exposure at 1.6 MHz and 0.5 MHz. More harmonic peaks were seen during insonation at 1.6 MHz, whereas greater broadband frequency content was seen during insonation at 0.5 MHz.

4. Discussion

4.1. Comparison of predictions and results

When comparing the computational and experimental results it can be seen that the model predicts almost negligible penetration distances in the non-cavitation regime. However in practice, cavitation activity was detected even without artificially introduced cavitation nuclei. The peak power of cavitation emissions measured using the passive cavitation detection (PCD) transducer was found to be $0.0002 \text{ mV}^2 \Omega^{-1}$ at baseline, and raised to $0.0016 \text{ mV}^2 \Omega^{-1}$ and $0.0120 \text{ mV}^2 \Omega^{-1}$ when the sample was exposed to 1.6 MHz and 0.5 MHz respectively. As expected, peak cavitation power was significantly greater when SV microbubbles were introduced, reaching $0.2404 \text{ mV}^2 \Omega^{-1}$ and $0.7361 \text{ mV}^2 \Omega^{-1}$ at 1.6 MHz and 0.5 MHz,

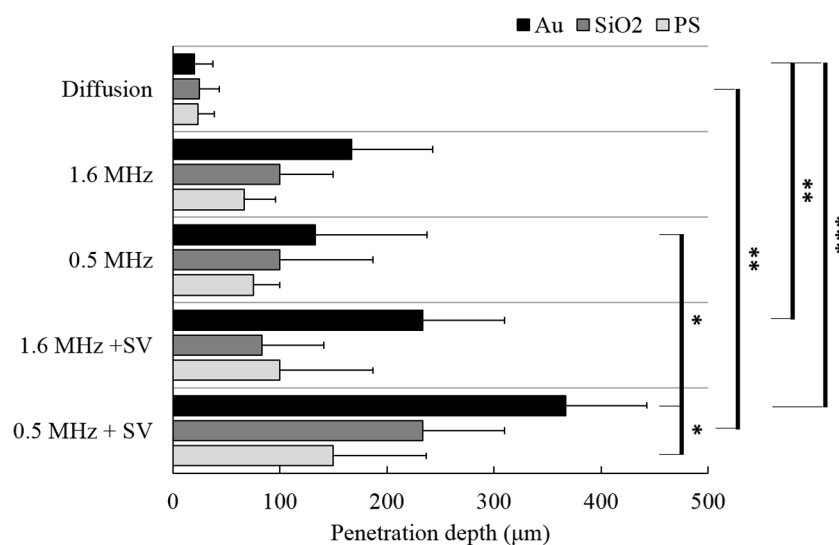


Figure 7. Penetration depths of density-contrasting particles under ultrasound exposure in four acoustic regimes. Statistical significance is assessed using one-way ANOVA testing: * ($p < 0.05$), ** ($p < 0.01$), *** ($p < 0.001$) where $n = 3$.

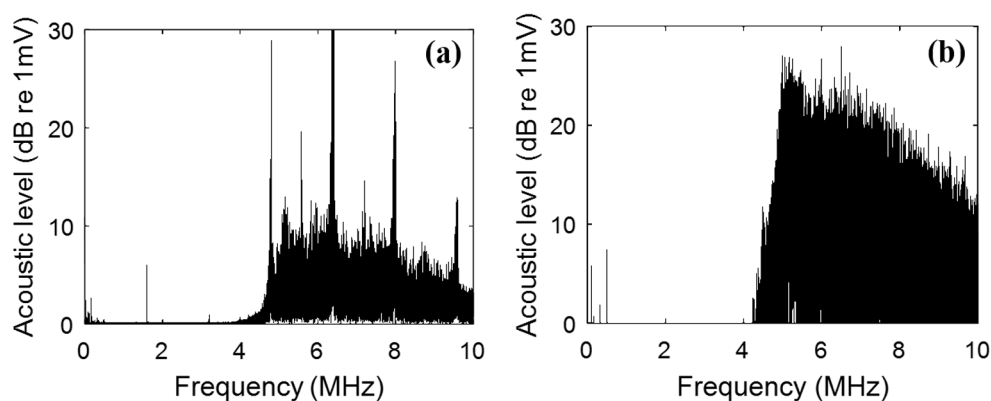


Figure 8. Fourier transforms of the passive cavitation detection (PCD) signals captured during exposure with SonoVue® microbubbles at 1 MPa and (a) 1.6 MHz and (b) 0.5 MHz.

respectively. Figure 8 shows the cavitation behaviour recorded during exposure using SV at 1.6 MHz and 0.5 MHz, with clear harmonic peaks present at 1.6 MHz and a broadband frequency response at 0.5 MHz.

Greater qualitative agreement for penetration depths is seen when computational predictions and experimental observations are compared in the cavitation regime, supporting the hypothesis that increasing particle density increases penetration depth. Furthermore, SV microbubbles excited at 0.5 MHz were both predicted and observed to induce greater particle transport than at 1.6 MHz.

It should be emphasised, however, that the computational model implemented in the current study is a substantial simplification of the true experimental conditions experienced by the suspended nanoparticle. Firstly, the simulation is only concerned with a

single-bubble-single-particle interaction, negating bubble–bubble or particle–particle interactions. In reality a population of microbubbles was observed, with a size distribution spanning a range of radii and resonant frequencies. Furthermore the nanoparticle is assumed to be rigid and sufficiently small that the scattered pressure field is negligible; therefore the incident pressure field is assumed to be unchanged by the presence of the particle.

The value of using a simple numerical model to predict ultrasound-mediated transport of nanoparticles has been shown in the context of elucidating the impact of nanoparticle density on penetration depth. In future work, however, it may be advantageous to add complexity to such a simulation, allowing the confines of a viscoelastic vasculature to be accounted for (Sassaroli *et al* 2005), rather than a free-field bubble, as well as bubble–bubble interactions (Parlitz *et al* 1999, Lauterborn *et al* 2010).

The tissue mimicking phantom, 1% concentration (wt%) agarose gel, was chosen because of its similar acoustic properties to tissue. The gel also has a porous structure, and at this concentration the pore size has been measured as ~200 nm (Narayanan *et al* 2006) which is in the range of pore sizes, 50–400 nm (Yuan *et al* 1995), observed between endothelial cells in cancerous vasculature. However, the homogeneity of this model must be acknowledged, and thus an agarose gel is inherently limited in representing the complex and chaotic structure of the cancerous tumour. Nevertheless, many studies have shown good agreement between *in vitro* experiments carried out in cell-embedded agarose phantoms and *in vivo* studies (Mo *et al* 2015). To enable translation into an *in vivo* context, further investigations using a more realistic vessel model to study the influence of particle density on ultrasound-mediated transport are recommended. Potential methods include using a dissected section of vessel or a tissue-engineered vascular graft (Mitchell *et al* 2003).

As discussed in the introduction, the results support the hypothesis that increased density played a significant role in enhancing the penetration depth of the modified adenovirus studied by Mo (2015). However, the potential applications of the current findings go beyond the field of virotherapy, arguably to all five major categories of tumour-targeted therapeutic—liposomal drug carriers, polymer-based carriers, micelles, solid nanoparticles (lipid-based, viral and ‘multistage’) and antibodies—by incorporating an inert, biocompatible dense metal, such as gold.

5. Conclusions

The overall conclusion of this study is that the penetration depth achieved by a nanoparticle under ultrasound exposure is significantly influenced by particle density. It has been shown that a denser particle will be transported further when exposed to ultrasound and cavitating microbubbles than its less dense counterpart. It has also been shown that exposing SonoVue® microbubbles to ultrasound at a frequency of 0.5 MHz induces greater nanoparticle transport than exposing at 1.6 MHz, due to the higher microstreaming velocities. Since limited penetration depth of nanoscale therapeutics is a current limitation in oncolytic drug delivery, these findings are important in designing density-modified drug carriers that can penetrate deep into cancerous tumours.

Acknowledgments

This research was funded by the Engineering and Physical Sciences Research Council (EPSRC) through the Oxford Centre for Drug Delivery Devices (OxCD³) grant number EP/L024012/1. The authors thank J Fisk and D Salisbury for manufacturing the phantom holders used in this work. Supporting data are available through the University of Oxford ORA data repository (doi: [10.5287/bodleian:PmBVRN8VX](https://doi.org/10.5287/bodleian:PmBVRN8VX)).

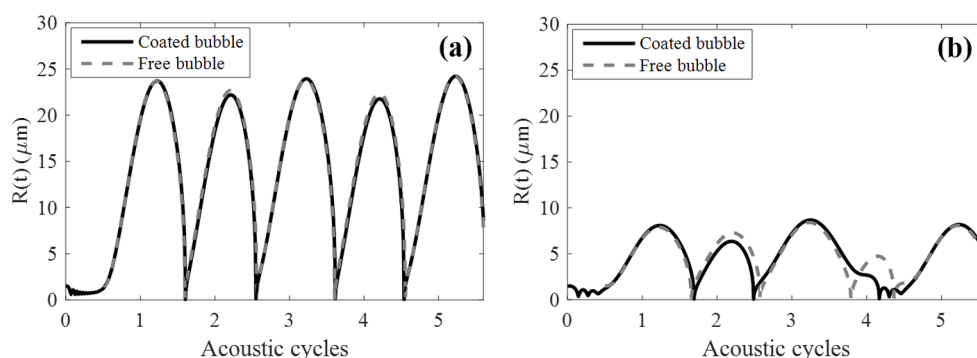


Figure A1. Simulated radius-time curves for a coated and free 3 μm bubble as determined by the Marmottant coated bubble model and the Keller–Miksis free bubble model respectively, driven at 1 MPa and (a) 0.5 MHz and (b) 1.6 MHz.

R_0	Equilibrium bubble radius	1.50 μm
R_{buckling}	Buckling bubble radius	1.50 μm
R_{ruptured}	Ruptured bubble radius ($R_{\text{ruptured}} = R_{\text{buckling}}(1 + \sigma_{\text{water}}/\chi)^{1/2}$)	1.50 μm
χ	Shell elasticity	1 N m^{-1}
κ_s	Shell friction ($\kappa_s = 3\mu_{\text{sh}}\varepsilon_{\text{sh}}$)	$15 \times 10^{-9} \text{ N}$
μ_{sh}	Shell viscosity	
ε_{sh}	Shell thickness	
$\sigma_{\text{break-up}}$	Maximum surface tension before rupture	$> 1 \text{ N m}^{-1}$
σ_{water}	Surface tension of water	0.072 N m^{-1}
κ	Polytropic gas exponent of SF_6	1.095
ρ_l	Liquid density	1000 kg m^{-3}
μ	Liquid viscosity	0.001 Pa s
c	Liquid sound speed	1480 m s^{-1}

Appendix. Dynamics of a coated and free microbubble

The amplitude of oscillation is predicted for a free bubble (as predicted by the Keller–Miksis equation) and for a coated bubble (as predicted by the Marmottant model). Figure A1 shows a comparison of oscillation amplitudes for a 3 μm bubble driven at 0.5 MHz or 1.6 MHz, at 1 MPa. The shell of the coated bubble is defined using experimentally derived parameters for a SonoVue[®] microbubble (Marmottant 2005) shown above. It can be seen that at these acoustic exposures this type of coating has very little influence on the amplitudes of oscillation.

References

- Bhatnagar S, Schiffter H and Coussios C C 2014 Exploitation of acoustic cavitation-induced microstreaming to enhance molecular transport *J. Pharm. Sci.* **103** 1903–12
- Blanco E, Shen H and Ferrari M 2015 Principles of nanoparticle design for overcoming biological barriers to drug delivery *Nat. Biotechnol.* **33** 941–51

- Carlisle R, Choi J, Bazan-Peregrino M, Laga R, Subr V, Kostka L, Ulbrich K, Coussios C C and Seymour L W 2013 Enhanced tumour uptake and penetration of virotherapy using polymer stealthing and focused ultrasound *J. Natl Cancer Inst.* **105** 1701–10
- Chen X, Yan Y, Müllner M, van Koeveerden M P, Noi K F, Zhu W and Caruso F 2014 Engineering fluorescent poly (dopamine) capsules *Langmuir* **30** 2921–5
- de Bruyn J R and Walsh A M 2004 Penetration of spheres into loose granular media *Can. J. Phys.* **82** 439–46
- Doinikov A A and Bouakaz A 2010 Acoustic microstreaming around a gas bubble *J. Acoust. Soc. Am.* **127** 703–9
- Dougherty T J and Marcus S L 1992 Photodynamic therapy *Eur. J. Cancer* **28** 734–1742
- Hobbs S K, Monsky W L, Yuan F, Roberts W G, Griffith L, Torchilin V P and Jain R K 1998 Regulation of transport pathways in tumor vessels: role of tumor type and microenvironment *Proc. Natl Acad. Sci.* **95** 4607–12
- Ilinskii Y A and Zabolotskaya E A 1992 Cooperative radiation and scattering of acoustic waves by gas bubbles in liquids *J. Acoust. Soc. Am.* **92** 2837–41
- Kamaly N, Xiao Z, Valencia P M, Radovic-Moreno A F and Farokhzad O C 2012 Targeted polymeric therapeutic nanoparticles: design, development and clinical translation *Chem. Soc. Rev.* **41** 2971–3010
- Keller J B and Miksis M 1980 Bubble oscillations of large amplitude *J. Acoust. Soc. Am.* **68** 628–33
- Lauterborn W and Kurz T 2010 Physics of bubble oscillations *Rep. Prog. Phys.* **73** 1–88
- Lübbe A S, Alexiou C and Bergemann C 2001 Clinical applications of magnetic drug targeting *J. Surg. Res.* **95** 200–6
- Maaloum M, Pernodet N and Tinland B 1998 Agarose gel structure using atomic force microscopy: gel concentration and ionic strength effects *Electrophoresis* **19** 1606–10
- Maeda H 2010 Tumor-selective delivery of macromolecular drugs via the EPR effect: background and future prospects *Bioconjug. Chem.* **21** 797–802
- Marmottant P, van der Meer S, Emmer M, Versluis M, de Jong N, Hilgenfeldt S and Lohse D 2005 A model for large amplitude oscillations of coated bubbles accounting for buckling and rupture *J. Acoust. Soc. Am.* **118** 3499–505
- Minchinton A I and Tannock I F 2006 Drug penetration in solid tumours *Nat. Rev. Cancer* **6** 583–92
- Mitchell S L and Niklason L E 2003 Requirements for growing tissue-engineered vascular grafts *Cardiovasc. Pathol.* **12** 59–64
- Mo S, Carlisle R, Laga R, Myers R, Graham S, Cawood R, Ulbrich K, Seymour L and Coussios C-C 2015 Increasing the density of nanomedicines improves their ultrasound-mediated delivery to tumours *J. Control. Release* **210** 10–8
- Mo S, Coussios C C, Seymour L and Carlisle R 2012 Ultrasound-enhanced drug delivery for cancer *Expert Opin. Drug Deliv.* **9** 1525–38
- Narayanan J, Jun-Ying X and Xiang-Yang L 2006 Determination of agarose gel pore size: absorbance measurements vis a vis other techniques *J. Phys.: Conf. Ser.* **28** 83–6
- Parlitz U, Mettin R, Luther S, Akhatov I, Voss M and Lauterborn W 1999 Spatio-temporal dynamics of acoustic cavitation bubble clouds *Phil. Trans. R. Soc. A* **357** 313–34
- Popović Z, Liu W, Chauhan V P, Lee J, Wong C, Greytak A B, Insin N, Nocera D G, Fukumura D, Jain R K and Bawendi M G 2010 A nanoparticle size series for *in vivo* fluorescence imaging *Angew. Chem.* **122** 8831–4
- Prabhakar U, Maeda H, Jain R K, Sevick-Muraca E M, Zamboni W, Farokhzad O C, Barry S T, Gabizon A, Grodzinski P and Blakey D C 2013 Challenges and key considerations of the enhanced permeability and retention effect for nanomedicine drug delivery in oncology *Cancer Res.* **73** 2412–7
- Sassaroli E and Hynynen K 2005 Resonance frequency of microbubbles in small blood vessels: a numerical study *Phys. Med. Biol.* **50** 5293–305
- Schneider M, Arditi M, Barrau M B, Brochot J, Broillet A, Ventrone R and Yan F 1995 BR1: a new ultrasonographic contrast agent based on sulfur hexafluoride-filled microbubbles *Invest. Radiol.* **30** 451–7
- Wilhelm S, Tavares A J, Dai Q, Ohta S, Audet J, Dvorak H F and Chan W C 2016 Analysis of nanoparticle delivery to tumours *Nat. Rev. Mater.* **1** 1–12
- Yuan F, Dellian M, Fukumura D, Leunig M, Berk D A, Torchilin V P and Jain R K 1995 Vascular permeability in a human tumor xenograft: molecular size dependence and cutoff size *Cancer Res.* **55** 3752–6 (<http://cancerres.aacrjournals.org/content/55/17/3752.full-text.pdf>)